Chapter 7

Stability Landscape of Aliovalent Cation Substituted (Fe,Co,Ni,Cu,Zn)O High Entropy Oxide for Oxygen Evolution Reaction

7.1 Introduction

The depletion of non-renewable fossil fuels and accompanying environmental difficulties, like global warming, provide significant challenges for humanity. There is a great need to create sustainable and renewable energy sources. Electrocatalysis [269] is a potential energy storage and conversion technology that uses renewable resources such as solar and wind power to create clean fuels and high-value compounds like hydrogen, ammonia, and ethylene. The sluggish oxygen evolution reaction (OER) with four-electron transfer poses a significant problem in electrochemical water splitting demanding the establishment of effective and stable electrocatalysts to lower the OER reaction barrier [166,270]. Several electrocatalysts have been developed to overcome the kinetic barrier of oxygen evolution reaction (OER) Traditional catalysts, including noble metals like platinum (Pt) and iridium (Ir), although effective but suffer from scarcity and high costs [162]. Transition metal oxides (*3d* TMOs) are potential alternatives for noble metal-based catalysts; however, less active sites limit their practical applications and there is still room for improvement in their intrinsic activities [201]. High entropy oxides (HEOs) [151] represent a burgeoning class of materials

characterized by their configurational entropy, leading to remarkable stability and diverse chemical functionalities. Recent studies have demonstrated the potential of HEOs as highly efficient electrocatalysts, offering a promising alternative to traditional cobalt (Co), nickel (Ni), and noble metal catalysts. Alkali metal cations such as Li^+ and Na^+ is strategically incorporated into rocksalt (Fe,Co,Ni,Cu,Zn)O HEOs for both stabilization and enhancement of OER kinetics. Due to their monovalent nature, the substitution of Li^+ or Na^+ for the divalent TM cations introduces a local charge imbalance, which is compensated by the formation of oxygen vacancies and some of the cations taking up a higher valence state. The vacancies help in relieving lattice strain and increasing the configurational entropy, thereby stabilizing the rocksalt phase.

Five component rocksalt (Mg,Co,Ni,Cu,Zn)O HEO was synthesized for the first time in 2015 via a solid-state method [22]. Subsequently, several research groups synthesised and examined a range of high-entropy oxides for various applications [153,166,169]. HEOs can form in a variety of crystal structures due to their ability to stabilize a single-phase solid solution despite the inclusion of multiple cations in near-equimolar proportions [46]. Some of the common structures observed in HEOs include rocksalt [16,237,271,272], spinel [26,29,65,185], perovskite [37–41] and fluorite [32–35]. Constituent elements in these structures significantly influence the physical and chemical properties of the HEOs, especially in their application as electrocatalysts. HEOs have shown significant promise in catalysing OER due to their tunable surface properties and the ability to incorporate multiple active sites. The presence of mixed valence states and oxygen vacancy concentrations promotes

the adsorption of oxygen intermediates, thereby accelerating the reaction kinetics. The multicomponent nature of HEOs leads to synergistic effects, where the interaction between different cations enhances catalytic performance beyond the individual contributions of each metal. This synergy can be optimized by selecting elements with complementary electronic and chemical properties, such as combining redox-active and oxygen-stabilizing cations. In an early effort to explore HEO as electrocatalysts [57,62], Wang et al. [28] synthesized a spinel-structured $(Co,Cu,Fe,Mn,Ni)_3O_4$ using a low-temperature solvothermal technique and tested it for OER which highlights the variety of valence states and chemical constituents in HEO generates several intermediates, facilitating the circumvention of kinetic barriers more effectively than mixed metal oxides with fewer elements. They showed HEO responds OER with a Tafel slope of 59.5mV dec^{-1}. In another study, Liu et al.[24] reported OER activity at an overpotential of 360 mV dec^{-1} to reach 10mAcm^{-2} current density for (Mg,Co,Ni,Cu,Zn)O HEO synthesized via electrospinning, which was quite lower compared to their constituent oxides. They attributed these findings to the strengthening of Co/Ni-O covalency and lattice mismatch due to the ionic size differences, which leads to oxygen vacancy. Thus, oxygen vacancies and synergistic effects play critical role in OER, as oxygen vacancies create unsaturated metal sites on the catalyst surface, which act as active sites for the adsorption and activation of reaction intermediates, such as OH^- and OOH^- [184,237]. This improves the kinetics of the OER. Moreover, various reports indicate that the composition and methodological adjustments are also important factors for electrocatalytic characteristics [168,169,201,273–275]. In

(Mg,Co,Ni,Cu,Zn)O R-HEO Mg^{2+}, Zn^{2+} are often considered inactive in catalytic reactions.

In this chapter, synthesis of phase pure rocksalt (Fe,Co,Ni,Cu,Zn)O HEO using the SCS route and the effect of Na^{1+} and Li^{1+} substitution on the phase stability of the rocksalt phase is discussed. Subsequently Li^{1+} and Na^{1+} substituted rocksalt phase was evaluated for its electrocatalyst of OER.

7.2 Experimental details

These metal nitrates were utilized as precursors to synthesize nanocrystalline (Fe,Co,Ni,Cu,Zn)O, (Fe,Co,Ni,Cu,Zn,Li)O and (Fe,Co,Ni,Cu,Zn,Na)O powders by (SCS) technique (already explained in chapters 3 and 4). After the combustion as synthesis calcination was carried and followed by quenching in air. For single phase rocksalt (Fe,Co,Ni,Cu,Zn)O HEO calcination temperature was 1200°C whereas for (Fe,Co,Ni,Cu,Zn,Li)O, and (Fe,Co,Ni,Cu,Zn,Na)O it was 1050°C. Hereafter, the equiatomic compositions (Fe,Co,Ni,Cu,Zn)O, (Fe,Co,Ni,Cu,Zn, Li)O, and (Fe,Co,Ni,Cu,Zn,Na)O will be referred to as HEO-5, HEO-6A, and HEO-6B, respectively.

To prepare the working electrode for the oxygen evolution reaction, 7 mg HEO and 2 mg graphene powders were dispersed in 340 µL water and 150 µL IPA and sonicated for 60 min. Subsequently, 40 µL of Nafion (5%) solution was added as a binder and the mixture was again sonicated for 10 min to obtain a homogeneous ink. 250 µL of the prepared ink was drop cast on a $1cm^2$ carbon paper and vacuum dried for 100 °C to prepare the electrode. for oxygen evolution reaction. Ag/AgCl

was used as a reference electrode while Pt wire was used as the counter electrode. All three electrodes were immersed in 1M KOH electrolyte in the cell. Electrocatalytic tests were performed using three electrode measurement setups with AUTOLAB NOVA in the potential range of 1.1 to 1.9 V vs RHE. The OER overpotential was calculated by linear sweep voltammetry (LSV) at a scan rate of 5 mVs^{-1}. Electrochemical impedance spectroscopy was performed at 1.6 V at the frequency range of 0.1 MHz to 0.1 Hz and amplitude of 0.01. The potentials measured (versus Ag/ AgCl) were calibrated relative to RHE and were processed using the following calculation:

$$E_{RHE} = E_{Ag/AgCl} + 0{:}059 \times pH + 0{:}197 \qquad (1)$$

Whrere pH of KOH = 13.7 at room temperature.

$$\text{Overpotential } (\eta) = E_{RHE} - 1.23 \qquad (2)$$

7.3 Results and discussion

7.3.1 XRD and morphological analysis

To examine the phase purity and crystal structure of synthesized and annealed (at 1200 ℃ for HEO-5 and 1050℃ for HEO6A and HEO6B) HEO powder samples, X-ray diffraction (XRD) was performed. The obtained XRD patterns reveal the presence of sharp and well-defined peaks corresponding to (111), (200), (220), (311), (222) planes of a single- phase rocksalt structure (space group $Fm\bar{3}m$) with no evidence of secondary phases within the detection limit of the instrument,

suggesting that the entropy term (TΔS) was more than enough to compensate for the enthalpy of mixing (ΔH_{mix})[45,52,151].

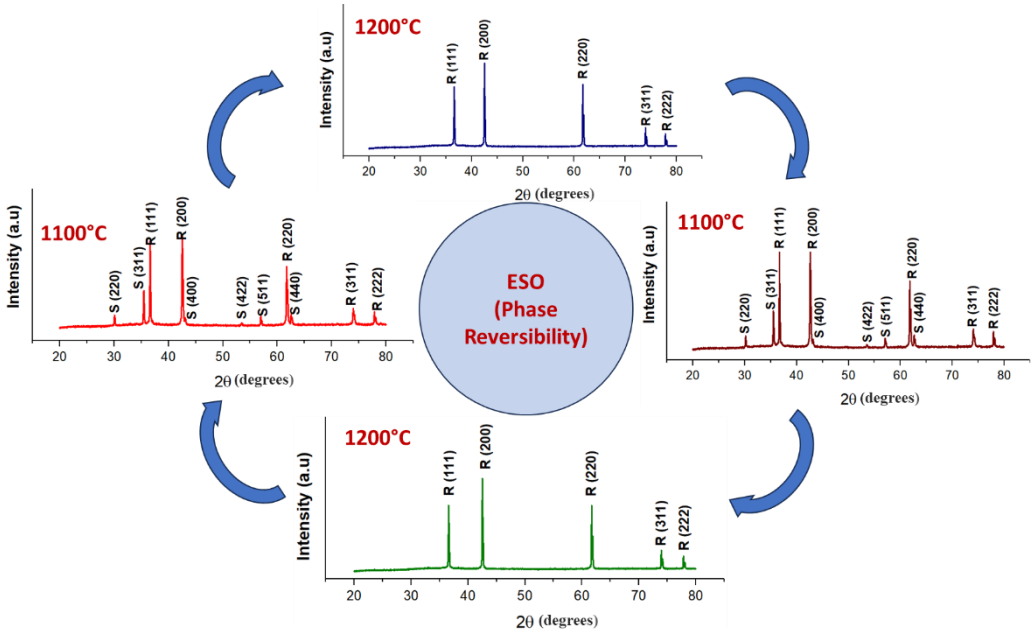

Figure 7.1 XRD pattern shows mixed phase (rocksalt and spinel) at temperature1100°C, which transformed to single phase rocksalt structure at 1200°C. when temperature reversed back to 1100 °C again spinel phase appears along with rocksalt phase.

Rietveld analysis was performed using GSAS II software suite to obtain the lattice parameter (a), the primary crystallite size (D) and micro-strain (ε), and listed in **Table 7.1**. XRD pattern recorded for HEO-5 annealed at 1100 ℃ shows two distinct phases: rocksalt and spinel, however, on annealing at 1200 ℃, a single rocksalt phase is obtained (**Figure 7.1**). This indicates that, at 1100 ℃, the TΔS term was not sufficiently high to compensate for the enthalpy of mixing ΔH_{mix}, while somewhere between 1100-1200 ℃ entropy stabilization of single rocksalt phase

takes place as evident from the XRD pattern obtained at 1200 ℃. The tendency of spinel in HEO-5 is understandable from the fact that out of 5 components Co, Fe, and Ni can assume both +2 and +3 oxidation states and can form spinel [16]. Various reports suggest that Co_3O_4 and Fe_2O_3 spinel phase decomposes to CoO, and FeO and assumes a rocksalt phases on heating to higher temperatures [23,271,276]. In addition, phase reversibility is also noticed in HEO5 samples on thermal cyclic between 1100℃ and 1200℃, as shown in **Figure 7.1**, which clearly indicates that the stabilization of rocksalt was primarily due to the entropy term, similar to the earlier reports on (Mg,Co,Ni,Cu,Zn)O HEO.

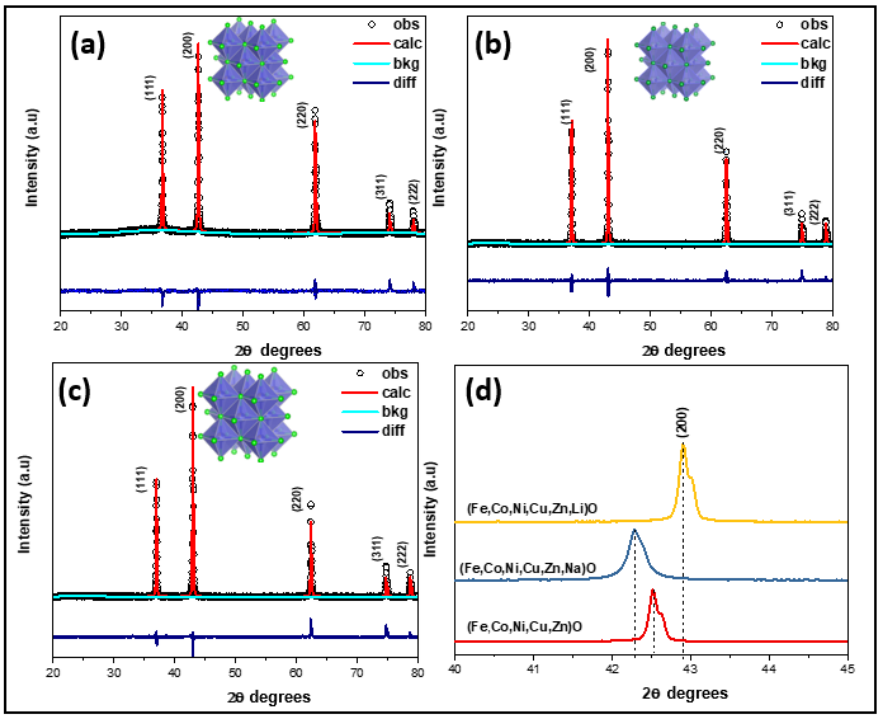

Figure 7.2 XRD pattern of (a) HEO-5 (b) HEO-6A (c) HEO-6B indicating single phase rocksalt structure (d) high intensity peak shifting indicate change in lattice parameter for six component HEO compared to quinary HEO.

In the case of HEO-6A and HEO-6B samples, single phase rocksalt structure formed at 1050 °C indicating that the addition of an aliovalent ions (Li^{1+}, Na^{1+}) as sixth element promotes rocksalt phase at comparatively lower temperatures than HEO-5[277]. It is obvious that the addition of the sixth element increases configurational entropy and TΔS; however, both Na and Li are larger than the average size of the parent composition (HEO-5) and have +1 valency, which is different from the +2 valency of ions in rocksalt structure. Therefore, if Li and Na goes into the regular cationic site in the rocksalt unit cell with +1 valency, it will introduce strain, and the unit cell will not be charge neutral [56,81,114]. The strain energy will add to the enthalpy term while the charge imbalance can be addressed through one of the charge compensation mechanisms [19,49,203], such as the creation of vacancies and some other ions assuming +3 state, which again requires energy and would be added to the enthalpy term. Therefore, rocksalt structure will be stabilized above a temperature where the increased enthalpy is more than compensated by the entropy term (-TΔS). The XRD patterns (**Figures 7.1b,** and **c**) suggest that the critical temperature for the Li and Na added HEOs (HEO-6A and HEO-6B) is lower than HEO-5 and single phase rocksalt is observed at 1050 °C.

Table 7.1 lattice parameter (*a*), crystallite size (D), and microstrain (ε) obtained from XRD Rietveld analysis.

Sample	*a* (Lattice parameter) A°	D (Crystallite size) nm	ε (Microstrain) %
HEO-5	4.241 ± 0.003	44	0.59
HEO-6A	4.203 ± 0.002	33	0.42
HEO-6B	4.249± 0.003	37	0.36

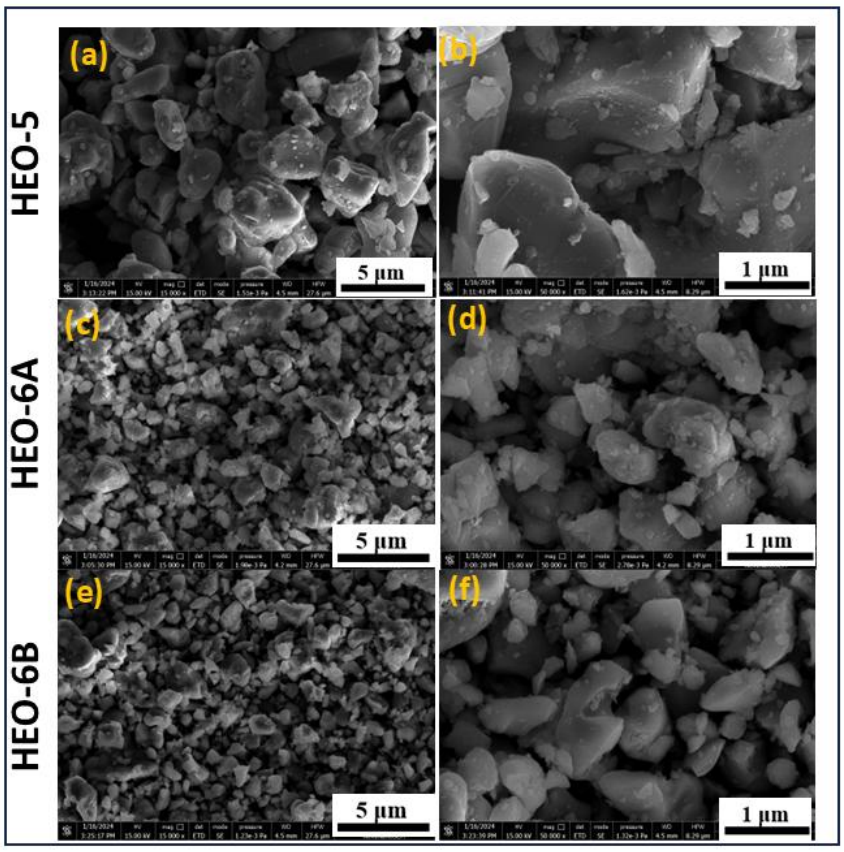

Figure 7.3 Morphology of synthesized HEO-5, HEO6A and HEO-6B.

To analyse the morphology and microstructure of HEOs, scanning electron microscopy was performed. SEM images of the HEO powders (shown in **Figure 7.3**) reveal larger agglomerates, which were made of primary particles of sizes calculated from XRD. Larger agglomerates of the orders of 1.2 µm are observed in HEO-5, which is greater than 0.6 µm and 0.8µm for HEO-6A and HEO-6B, respectively. The larger size of agglomerate formation in the case of HEO-5 is due to the higher annealing temperature (1200 ℃) when compared to 1050℃ for HEO-6A and HEO-6B, respectively. The elemental EDS maps of powders, shown in **Figure 7.4**, confirm the uniform distribution of all the constituent elements.

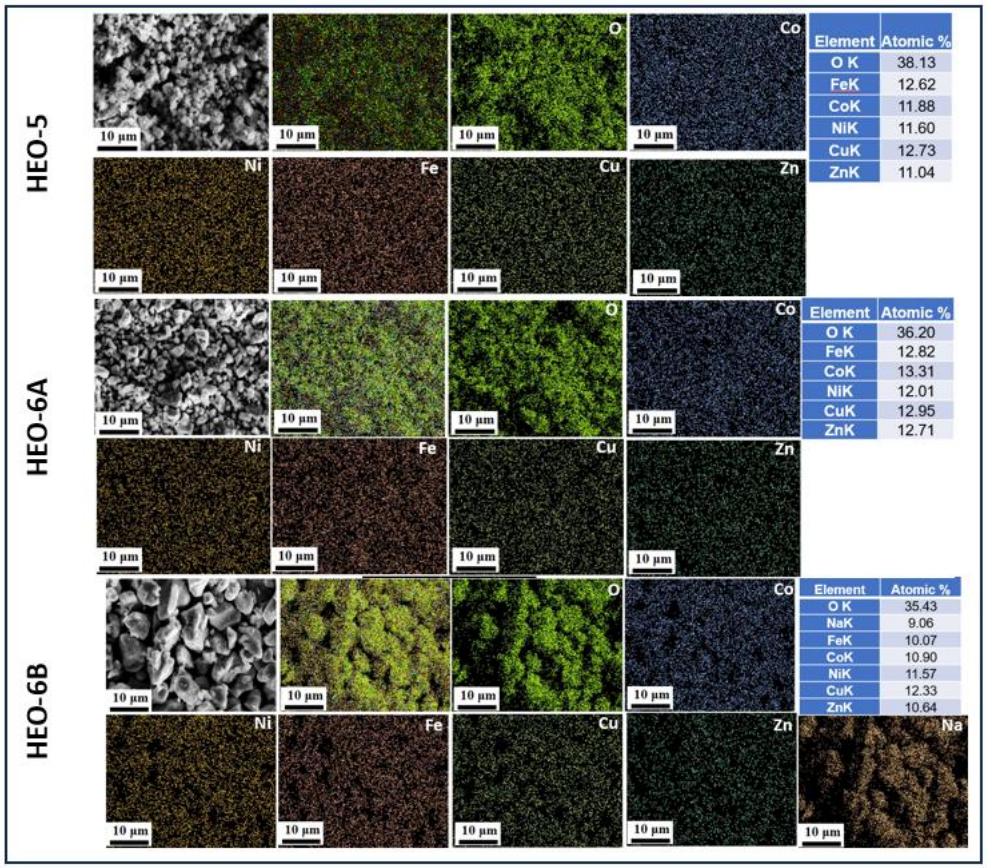

Figure 7.4 Elemental mapping and EDS of (a) HEO-5 (b) HEO-6A (c) HEO-6B confirms uniform distribution.

7.3.2 XPS analysis

To unveil the role of individual cations in charge compensation for stabilizing the rocksalt structure, X-ray photoelectron spectroscopy (XPS) analysis was carried out. **Figure 7.5** shows the core level spectra of the elements present in HEO-5. The high-resolution Co *2p* spectrum could be deconvoluted into four distinct peaks, including two primary peaks centred around 780.7 eV and 796.9 eV attributed to Co $2p_{3/2}$, $2p_{1/2}$, respectively; while the other two peaks at 784.74 eV and 803.31 eV correspond to the satellite peaks. Further, the fit Co *2p* revealed the presence of Co in +2 and +3 oxidation states in a $Co^{3+}/_{Co^{2+}}$ ratio ≈ 0.45. Similarly, the main peaks of the high-resolution XPS scan of Ni *2p* could be deconvoluted into two sets of spin-orbit doublets attributed to Ni^{2+} and Ni^{3+} which is accompanied by two shakeup satellite peaks. $Ni^{3+}/_{Ni^{2+}}$ ≈ 0.39 was obtained from fitting, revealing that a comparatively lower fraction of Ni is present in +3 oxidation state than Co. The peak at 934.2 eV and 954.7 eV is ascribed to Cu $2p_{3/2}$ and Cu $2p_{1/2}$, which could be deconvoluted into +2 and +1 oxidation states, respectively, with $Cu^{1+}/_{Cu^{2+}}$ ratio ≈ 0.3. The high-resolution Fe *2p* spectra reveal prominent Fe $2p_{3/2}$ and Fe $2p_{3/2}$ peaks accompanied by distinctive shakeup satellite features at higher energies, while the Fe $2p_{3/2}$ binding energy range of 710.8-711.5 eV confirms the coexistence of Fe^{2+} and Fe^{3+} oxidation states with $Fe^{3+}/_{Fe^{2+}}$ ratio≈0.39. In the high-resolution O 1s scan of the HEO, the peak at 529.6 eV is characteristic of metal–oxygen (M-O) bonds, while the peak at 531.8 eV indicates under-coordinated oxygen[81]. The wide scan of Zn 2p reveals two distinct peaks at binding energies of approximately 1021.3 eV (Zn $2p_{3/2}$) and 1044.4 eV (Zn $2p_{1/2}$), with splitting energy of 23.1 eV

consistent with divalent Zn oxides, confirming the +2 oxidation state. Similarly, the Mg *1s* spectral peak at around 1304.4 eV highlights its +2 valence state in the HEO.

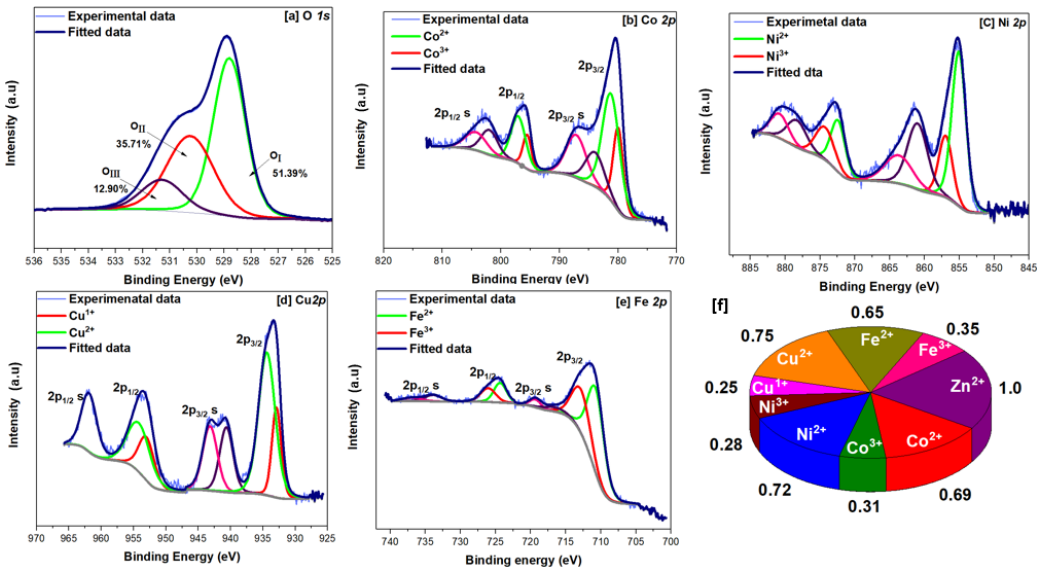

Figure 7.5 XPS survey scan of (a) O1s (b) Co 2p (c) Ni 2p (d) Cu 2p (e) Fe 2p in HEO-5 (f) schematic showing fraction of element in different oxidation states.

Further, the addition of Li and Na as the sixth element in five component HEO results in a change in stoichiometry. It was earlier reported that the lattice parameter shows a strong dependency on lithium concentration, decreasing significantly as Li content increases [59]. In this case, the lattice parameter decreased to 4.203 ± 0.002 Å on lithium addition, while the ionic radius of Li^{1+} in an octahedral environment is larger than that of any M^{2+} cations in the material, this reduction aligns with a charge compensation mechanism, likely involving the oxidation of some M^{2+} (divalent) cations (such as cobalt or nickel) to M^{3+} (trivalent) or the formation of oxygen vacancies [63], which was also confirmed by XPS analysis (**Figure 7.6**) of Li added HEO (HEO-6A). High-resolution Co 2p scan indicates that the fraction of

Co in +3 oxidation state increased significantly due to Li^{1+} substitution and $Co^{3+}/_{Co^{2+}}$ ratio ≈2.7 is obtained from fitting. To accommodate the large size cation with +1 oxidation state (Na^{1+} in this case), oxidation of multivalent cations such as Co, Ni, Fe and creation of oxygen vacancy takes place [184]. However, it is observed that Ni and Fe respond less to the presence of aliovalent ions when compared to Co^{2+} as $Ni^{3+}/_{Ni^{2+}}$ *and* $Fe^{3+}/_{Fe^{2+}}$ ratios change marginally to around 0.71 and 0.67, respectively.

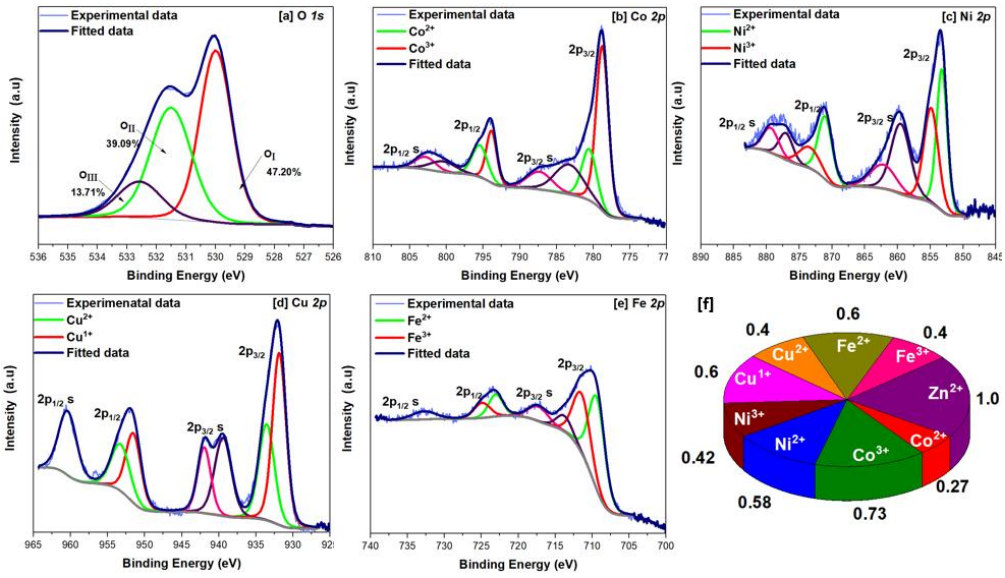

Figure 7.6 XPS survey scan of (a) O1s (b) Co 2p (c) Ni 2p (d) Cu 2p (e) Fe 2p in HEO-6A (f) schematic showing fraction of element in different oxidation state.

To maintain electrical neutrality in HEO system, Cu is present in both +1, and +2 oxidation state with $Cu^{1+}/_{Cu^{2+}}$ ratio ≈1.4. Moreover, oxygen deficit sites (O_v) increased on Li addition as estimated from the deconvolution of O1s peak (**Figure 7.6**). Similarly, in case of Na added HEO (HEO-6B), the larger size of the Na^{1+} is

compensated by increasing the fraction of both Co^{3+} and oxygen vacancy (**Figure 7.7**). **Table 7.2** highlights the ratios of different elemental valence states. The ionic size of Na^{1+} (1.07 Å) is greater than Li^{1+} and, therefore, generates a greater strain in the lattice which was compensated by creating defects. However, the fraction of multivalent cations in different oxidation states is nearly the same as in the HEO-6A sample as listed in **Table 7.2**.

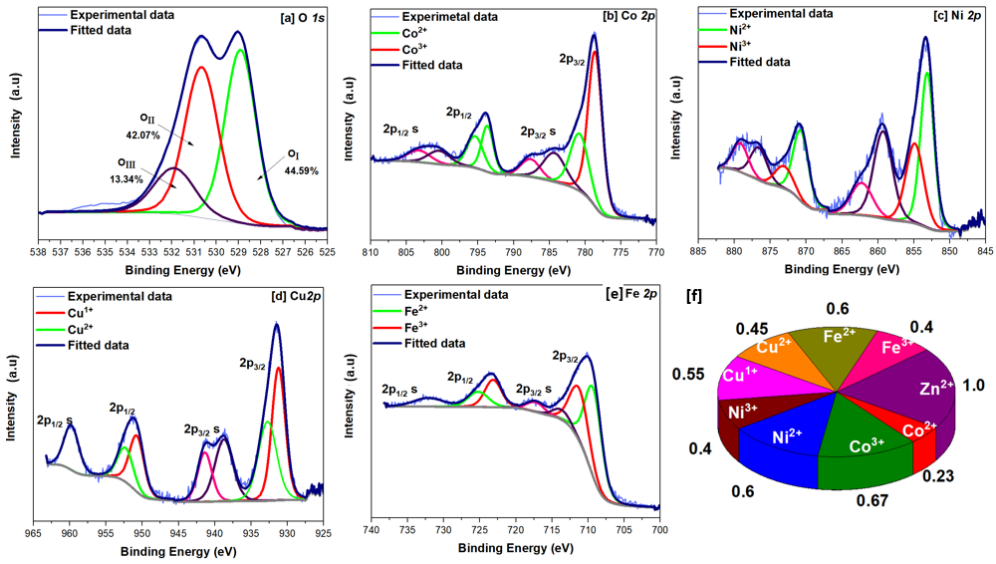

Figure 7.7 XPS survey scan of (a) O1s (b) Co 2p (c) Ni 2p (d) Cu 2p (e) Fe 2p in HEO-6B (f) schematic showing fraction of element in different oxidation state.

Table 7.2 Ratio of element in possible valence state due to charge compensation in HEO-5, HEO-6A and HEO-6B.

Sample	Co^{3+}/Co^{2+}	Ni^{3+}/Ni^{2+}	Cu^{1+}/Co^{2+}	Fe^{3+}/Fe^{2+}
HEO-5	0.45	0.39	0.3	0.39
HEO-6A	2.7	0.7	1.4	0.67
HEO-6B	2.9	0.67	1.2	0.67

7.3.3 Electrocatalytic oxygen evolution reaction (OER)

Transition metal oxides containing Fe, Co, and Ni have been extensively studied for their electrocatalytic activity in oxygen evolution reaction (OER) [57,153,177]. The synergetic interplay of these active elements in HEOs offer multiple active sites with broader charges ensuring dispersed *d* band centres and more continuous density of state near fermi level, which enable improved electrocatalytic OER when compared with unary oxides [24,278]. Therefore, the synthesized HEOs containing these elements have been evaluated for OER electrocatalytic activity. General mechanism of OER in an alkaline medium involves the transfer of 4 e^- in sequential reactions as follows [180,237,239]:

$$M + OH^- \longrightarrow M\text{-}OH + e^- \quad (1)$$
$$M\text{-}OH + OH^- \longrightarrow M\text{-}O + H_2O + e^- \quad (2)$$
$$M\text{-}O + OH^- \longrightarrow M\text{-}OOH + e^- \quad (3)$$
$$M\text{-}OOH + OH^- \longrightarrow M + O_2 + H_2O + e^- \quad (4)$$

where M is the active metal site, which reacts with the electrolyte (aqueous solution of KOH) to initially produce M-OH intermediates, which again combines with OH^- and produce intermediate M-O and H_2O. M-O then combines with OH^- and generates M-OOH, which decomposes to O_2. The free energy of these reactions determines the kinetics of OER [162,250,279]. **Figure 7.8a** shows the schematic of a general mechanism of OER using HEO as catalysts. **Figure 7.8b** compares the polarization curves of different synthesized rocksalt HEO in alkaline medium (1M KOH). Among these Li^{1+} added HEO (HEO-6A) exhibits a remarkably lower overpotential of 322 mV at 10 mA/cm^2 and Tafel slope of 63 mV/dec outperforming unary oxides (shown in **Figure 7.8c**), highlighting the synergistic enhancement

achieved through its multi-element composition [43,79,181]. Five component HEO and Na added HEO (HEO-6B) electrocatalysts showed overpotentials 415 mV and 395 mV, and Tafel slopes 92 mV/dec and 76 mV/dec, respectively. **Table 7.3** compares the OER response of the synthesised HEOs catalyst and unary oxides (CoO, and NiO) catalysts.

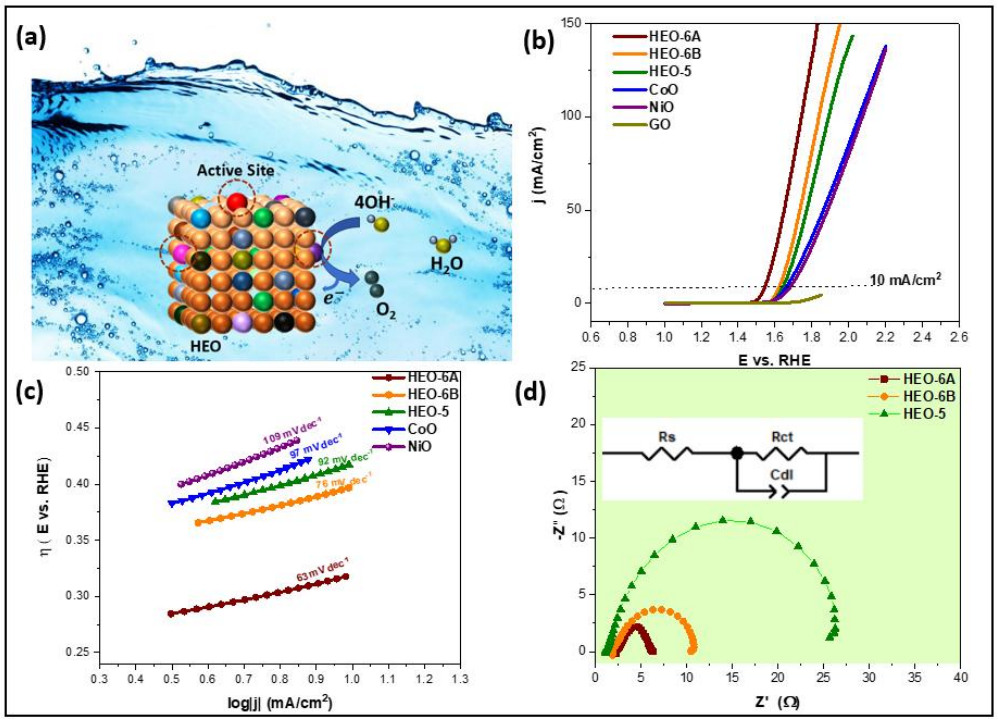

Figure 7.8 (a) Illustration of multiple active site and synergetic catalysis on HEO (b) LSV polarization curve (c) Tafel slope of synthesized HEO, CoO, NiO, and Graphene oxides (GO) (d) Nyquist plots recorded at 1.6V with equivalent circuit in the inset showing decreased charge transfer resistance (R_{ct}) for HEO-6A.

Jihyun [201] et al. analyzed individual role cations in (Co, Ni, Fe, Cr, Mn)O spinel HEO in which they reported that incorporating Fe provides a modest boost to activity, while the addition of Ni to Co, Fe significantly reduces the overpotential.

HEO shows enhanced OER performance owing to the synergistic effects of randomly mixed elements and the optimized adsorption energies. From the XPS (section 7.3.2), it is clear that diversity in the valence state and chemical components provides a large number of intermediates that can easily pass the energy barrier compared to unary metal oxides [277]. Li^{1+}, Na^{1+} in HEO-5 addition enhances Co/Ni-O covalency and density of vacancies, which provides larger

Table 7.3 Tafel slope, and overpotential (η_{10}) for different catalysis.

Sample	**Tafel Slope ($mVdec^{-1}$)**	**Overpotential mV (at 10 mA/cm^2)**
HEO-5	92	415
HEO-6A	63	322
HEO-6B	76	395
CoO	97	443
NiO	109	468

number of unsaturated active sites for reactant adsorption and electron transfer [184]. **Table 7.4** shows a comparison of OER activity reported for different HEOs. In addition, electrochemical impedance spectroscopy (EIS) measurements at 1.6V vs RHE reveal that the Li-added HEO (HEO-6A) exhibits the lowest charge transfer resistance at the catalyst-electrolyte interface when compared to HEO-5 and HEO-6B favouring interfacial charge transport between the active site and intermediates and valence states of elements and the overlap of multiple *d*-orbital increasing the density of state near the fermi energy level, which reduces charge transfer

Table 7.4 The reported Tafel slopes and overpotentials for HEOs electrocatalysts for OER in alkaline medium (KOH).

Catalysts	Electrolyte	Tafel slope ($mVdec^{-1}$)	Overpotential (mV) at 10 mA cm^{-2}	Ref
Pt nanowires	1 M KOH	-	520	[176]
(Co,Ni,Cu,Mg,Zn)O	1M KOH	68	360	[178]
(Co,Ni,Cu,Mg,Fe)O	1M KOH	70	430	[182]
$(Co,Ni,Mn,Zn,Fe)_3O_{3.2}$	1M KOH	-	366	[185]
$(CrMnFeCoNi)_3O_4$	1M KOH	65	366	[201]
(Fe,Co,Ni,Cu,Zn,Li)O	1M KOH	63	322	Present Work

resistance, thus highlighting its superior catalytic performance. **Table 7.5** lists the charge transfer resistance of synthesized HEOs during electrocatalysis. Overall improved activity of HEOs is ascribed to a larger density of active sites due to different valence states of elements and the overlap of multiple *d*-orbital increasing the density of state near the fermi energy level, which reduces charge transfer resistance in HEOs.

Table 7.5 Electrolyte resistance (R_s), charge transfer resistance (R_{ct}) for the synthesised HEO electrocatalysts.

Sample	**R_S (Ω)**	**R_{ct} (Ω)**
HEO-5	1.16	25.6
HEO-6A	1.87	6.3
HEO-6B	2.27	10.4

7.4 Conclusions

Five component (Fe,Co,Ni,Cu,Zn)O rocksalt HEO was synthesised via SCS. Incorporation of Li^{1+} and Na^{1+} promotes the phase stability of rocksalt structure. The addition of larger size cations (Li^{1+} and Na^{1+} in this case) results in oxidation of multivalent cation (mainly Co^{2+}), and creation of oxygen vacancies, thereby increasing Co/Ni-O covalency. The synthesized HEOs were evaluated as OER electrocatalysts, and their performance was compared. Li^{1+} added HEO (HEO-6A) exhibited the highest catalytic efficiency, achieving an impressively low overpotential of 322 mV at 10 mA/cm^2 and a Tafel slope of 63 mV/dec. This outstanding performance surpasses that of unary oxides such as CoO and NiO, underscoring the synergistic enhancements derived from its multi-element composition. This highlights the potential of high entropy oxides (HEOs) to be an efficient OER electrocatalyst, paving the way for their application in advanced energy conversion technologies.